

Supplementary material for "Kagome-like group-VA monolayers with indirect-direction band-gap transition and anisotropic mobility"

Jiajun Zhu¹, Chao He¹, Yong-Hong Zhao^{1,*} and Botao Fu^{1*}

¹ *College of Physics and Electronic Engineering, Center for Computational Sciences, Sichuan Normal University, Chengdu, 610068, China*

E-mail: yhzhao.cd@gmail.com; fubotao2008@gmail.com

The structural parameters and structural stabilities

Table S 1: The cohesive energy E_{coh} for different phosphorus allotropes are listed. Here we set the E_{coh} of α -P to be zero as the reference point. ^aThe data calculated from PBE level with the same computational parameters. ^bResults from Ref.[16], ^cresults from Ref.[19], ^dresults from Ref.[26], ^eresults from Ref.[18], ^fresults from Ref.[25], ^gresults from Ref.[22], ^hresults from Ref.[27].

Name	α -P	β -P	γ -P	δ -P	Ψ -P	λ -P
E_{coh} (eV/atom)	0.000 ^a	0.002 ^a	0.093 ^a	0.093 ^a	0.091 ^a	0.000 ^a
	0.00 ^b	0.00 ^b	0.09 ^b	0.08 ^b	0.09 ^c	0.000 ^d
Name	ξ -P	ε -P	kagome-P	α -P ₆	β -P ₆	<i>p</i> -Mono-(P ₂) _{cis}
E_{coh} (eV/atom)	0.085 ^a	0.148 ^a	0.120 ^a	0.141 ^a	0.092 ^a	0.306 ^a
	0.10 ^e	0.13 ^e	0.12 ^f	0.14 ^g	0.09 ^g	0.306 ^h

The cohesive energy for various phosphorus allotropes is comparatively shown in Tab. S1. We can see our results of known phosphorus allotropes are consistent with those from relevant references. Moreover, we find the α -P, β -P, γ -P, δ -P, Ψ -P, λ -P, ξ -P, β -P₆ have relatively lower

*To whom correspondence should be addressed

Table S 2: The detailed structural parameters for three kagome group-VA materials. \mathbf{a} is lattice constant, h is the interlayer height, $\theta_{1,2}$ and $l_{1,2}$ are bonding angle and length. The $\nu_{x/y}$ represents the Possion rate along x or y direction. The E_{coh} is the cohesive energy with respect to isolated atoms. Here we set the E_{coh} of α -phase to be zero as the reference point. The global band gap E_g and local band gap E_g^Γ at Γ point are calculated under HSE06 correction.

VA	\mathbf{a} (Å)	h (Å)	θ_1 (deg)	θ_2 (deg)	l_1 (Å)	l_2 (Å)	E_{coh} (eV/atom)	$\nu_{x/y}$	E_g (eV) (eV)	E_g^Γ (eV) (eV)
P	5.54	2.16	60	103.64	2.24	2.25	0.12	0.26/0.26	1.638	1.685
As	6.02	2.42	60	101.71	2.50	2.49	0.09	0.29/0.29	1.897	1.972
Sb	6.87	2.81	60	100.48	2.91	2.87	0.10	0.30/0.30	1.707	1.882

cohesive energy than that of kagome-P, while ϵ -P, α -P₆, p -Mono-(P₂)_{cis} have higher cohesive energy.

The structural parameters of kagome-P, As, Sb are listed in Tab. S2. The structural stabilities of kagome-As and Sb systems are verified by their phonon spectra and AIMD simulations as shown in Fig. S1. We can see there is no imaginary frequency in the whole Brillouin zone for both kagome-As and Sb, which indicates their dynamic stability. The AIMD simulations also confirm their thermodynamical stability under 300 K. In addition, higher temperature AIMDs are tested and we find that the crystal structures can be maintained until 800 K and 600 K for kagome-As and kagome-Sb, respectively.

The ferromagnetism induced by hole doping

Due to unique Mexican-hat-like valence band edges in kagome group-VA materials, they host almost diverging density of state below Fermi level. The electron instability under appropriate hole doping is explored and emergent ferromagnetism is revealed which can be explained by Stoner theory. We artificially simulate the hole doping process by removing out of the valence electrons on these systems and then calculate corresponding induced magnetic moment and spin polarization energy as shown in Figs. S2(a)-(c), where the spin polarization energy is defined as the energy difference between the nonmagnetic state and ferromagnetic state. For kagome-P, we find magnetic moment emerges at a very small hole concentration ($n=0.1 \times 10^{14} \text{ cm}^{-2}$) and rises straight

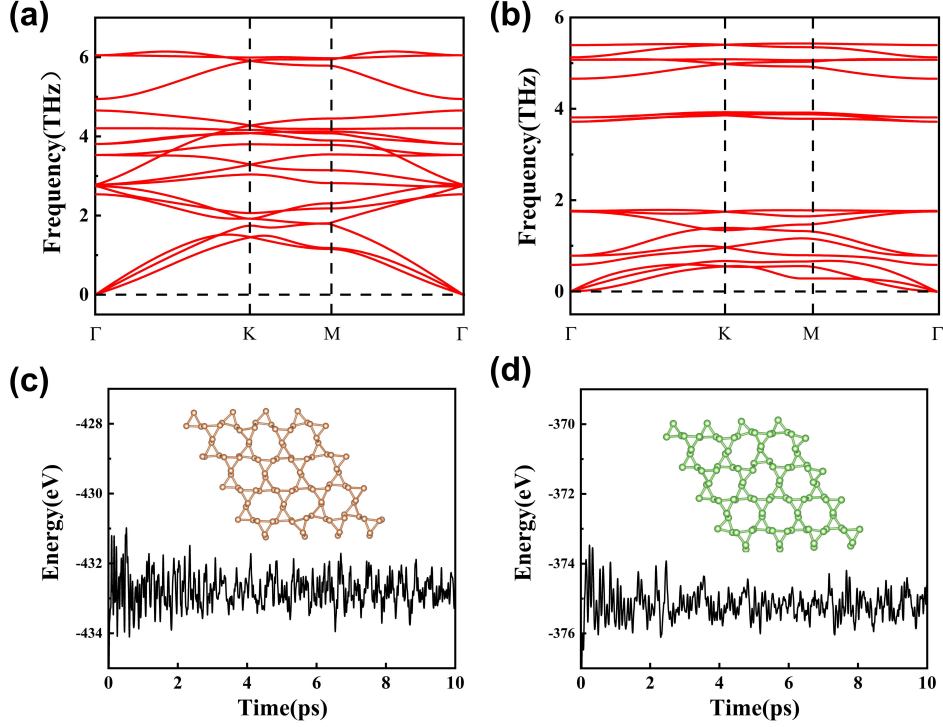


Figure S 1: The phonon spectra of kagome-As and Sb are displayed in (a) and (b), respectively. The total energy fluctuation during AIMD simulation under 300 K is shown in (c) and (d). A snapshot of crystal structure after 8 ps is given.

up to a saturation value of $1.0 \mu_B/\text{hole}$, which is maintained up to $n=2.0 \times 10^{14} \text{ cm}^{-2}$ and then descends rapidly to zero. While the spin polarization energy displays a positive peak in the whole doping range, which indicates the energy is favorable for the FM state. Similar results are found in kagome-As and Sb due to their similar electronic structures. The spin-polarized band structures of kagome-P at a moderate hole density $n=1.0 \times 10^{14} \text{ cm}^{-2}$ is shown in Fig. S2(d), which is a half-metal with 100% spin polarization with only the spin up channel across the Fermi level, and thus may has significant application in spintronics.

Strain engineering on bandstructures

The electronic structures of kagome-P under different strains are shown in Figs. S3(a)-(h). The indirect-direct band gap transition happens at the critical strain $\epsilon_x=3\%$ or $\epsilon_y=4\%$ as clearly shown in Figs. 3(c) and (g). Besides, we also investigate the strain effects on the electronic structures

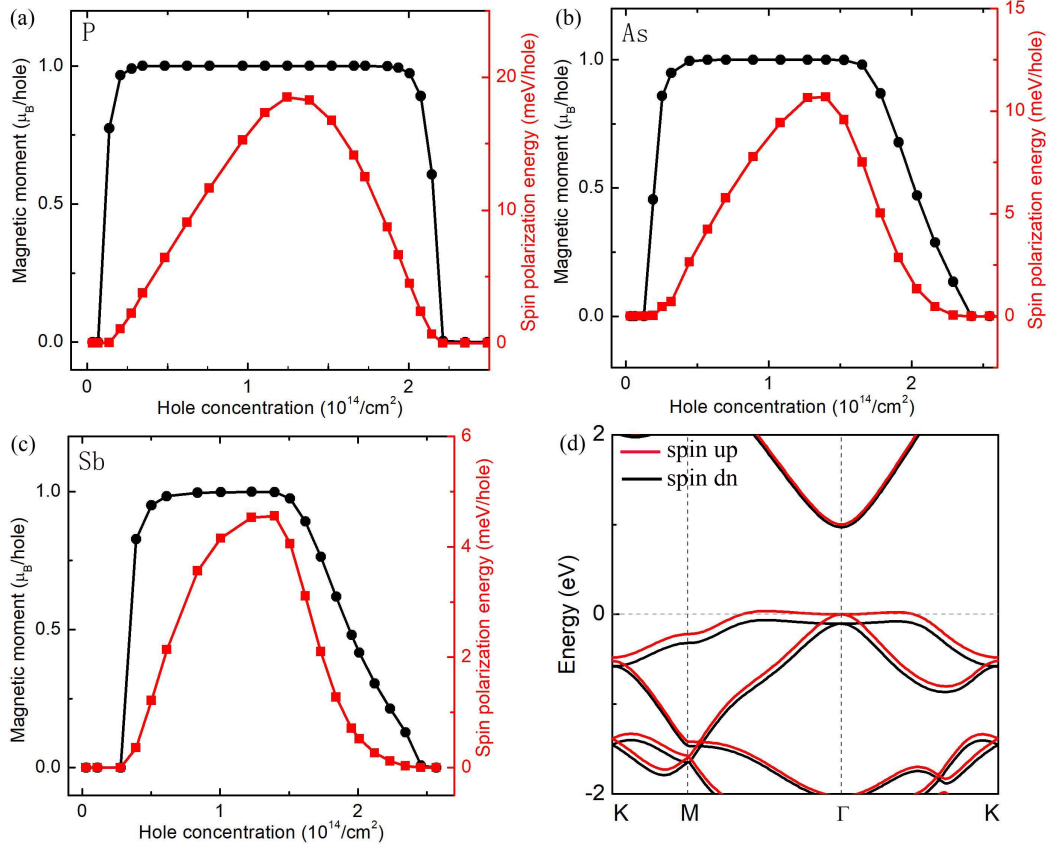


Figure S 2: (a)-(c) Magnetic moment and spin polarization energy versus hole doping concentration (n) for kagome-P, As and Sb, respectively. (d) The spin-polarized band structures of kagome-P is shown at $n=1.0 \times 10^{14} \text{cm}^{-2}$.

of kagome-As and Sb as shown in Figs. S3(i)-(x). Firstly, for both cases, the size of band gaps can be effectively tuned by both compressive and tensile strain akin to kagome-P. Secondly, like what happens in kagome-P, the indirect-direct band-gap transitions can also be triggered for both kagome-As and kagome-Sb under different critical strain values.

Other allotropes of group-VA elements

Based on an ab initio evolutionary crystal structure search method, various of crystal structures have been created. Except for the known allotropes such as α -P/ β -P and the kagome-P in this paper, we still find a new phase which has a close relation with kagome-P. We note it as tilted kagome-P. As shown in Fig. S4(a)-(c), starting from the substitution of two P-atoms in a hon-

eycomb lattice by two P-trimers, we obtain an initial configuration as a kagome lattice in Fig. S4(a). Now considering possible structural evolutions, each P-trimer has three degrees of freedom of translations (translation along x, y, z axes) as well as rotations. The potential constrains of stable three-coordination of each P-atom enables two P-trimers head to head and thus limit the degree of freedom. Firstly, the degree of translation along z will provide the buckling effect of two P-trimers and form a buckled kagome lattice, in Fig. S4(b). This structure is the center of our papers. Secondly, although rotation of z axis is greatly restricted, the rotation around x axis will provide the slanting effect of two-P trimers and form an new phase as shown in Fig. S4(c). We call it tilted kagome lattice. The structural stabilities of the tilted kagome-P, As, Sb are verified by the phonon spectra calculations in Fig. S4(d)-(f) and their band structures are demonstrated in Fig. S4(g)-(i).

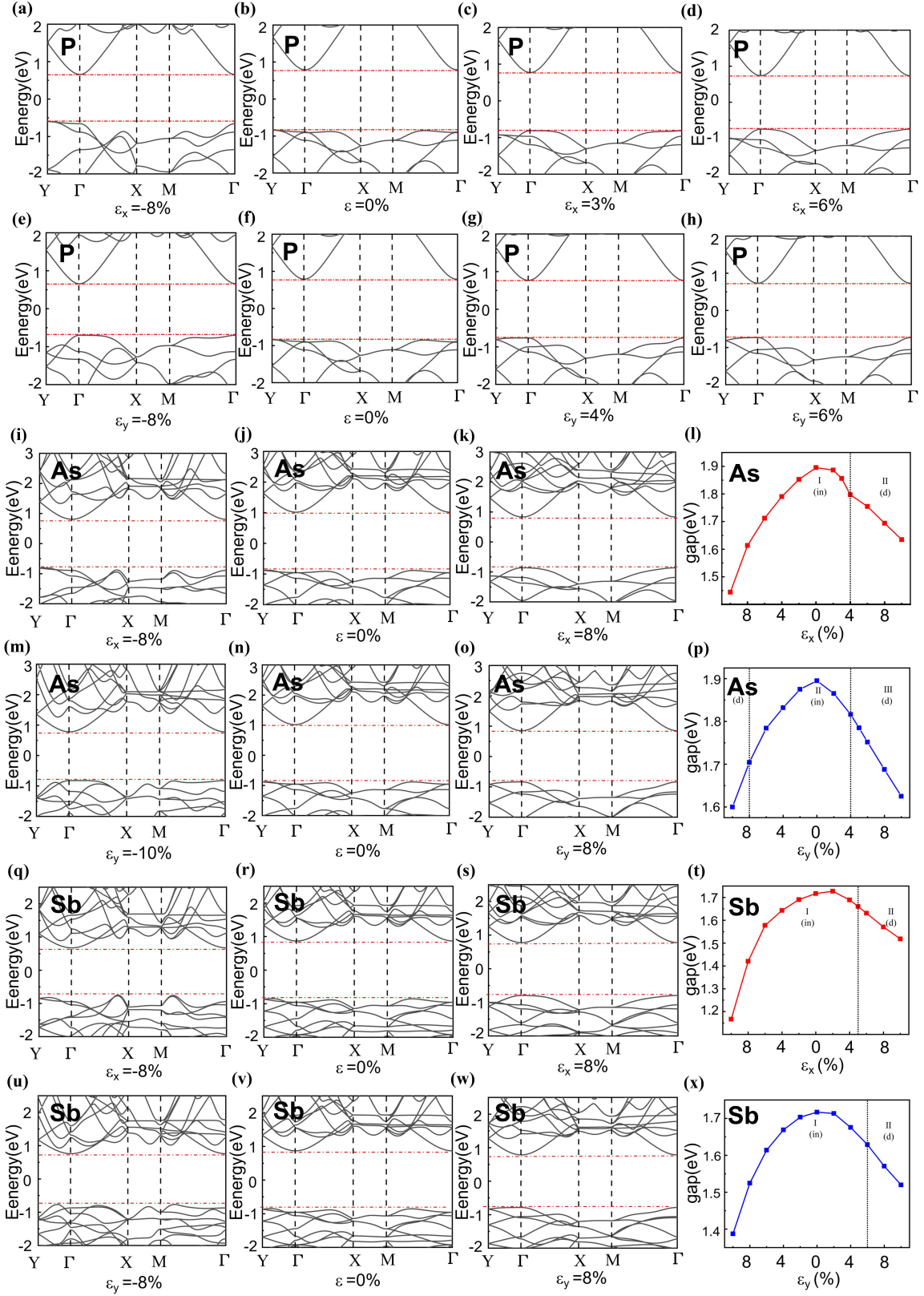


Figure S 3: Evolutions of the band structures of kagome-P, As and Sb under axial strains along x and y directions. The red dashed lines refer to the energy positions of CBM and VBM.

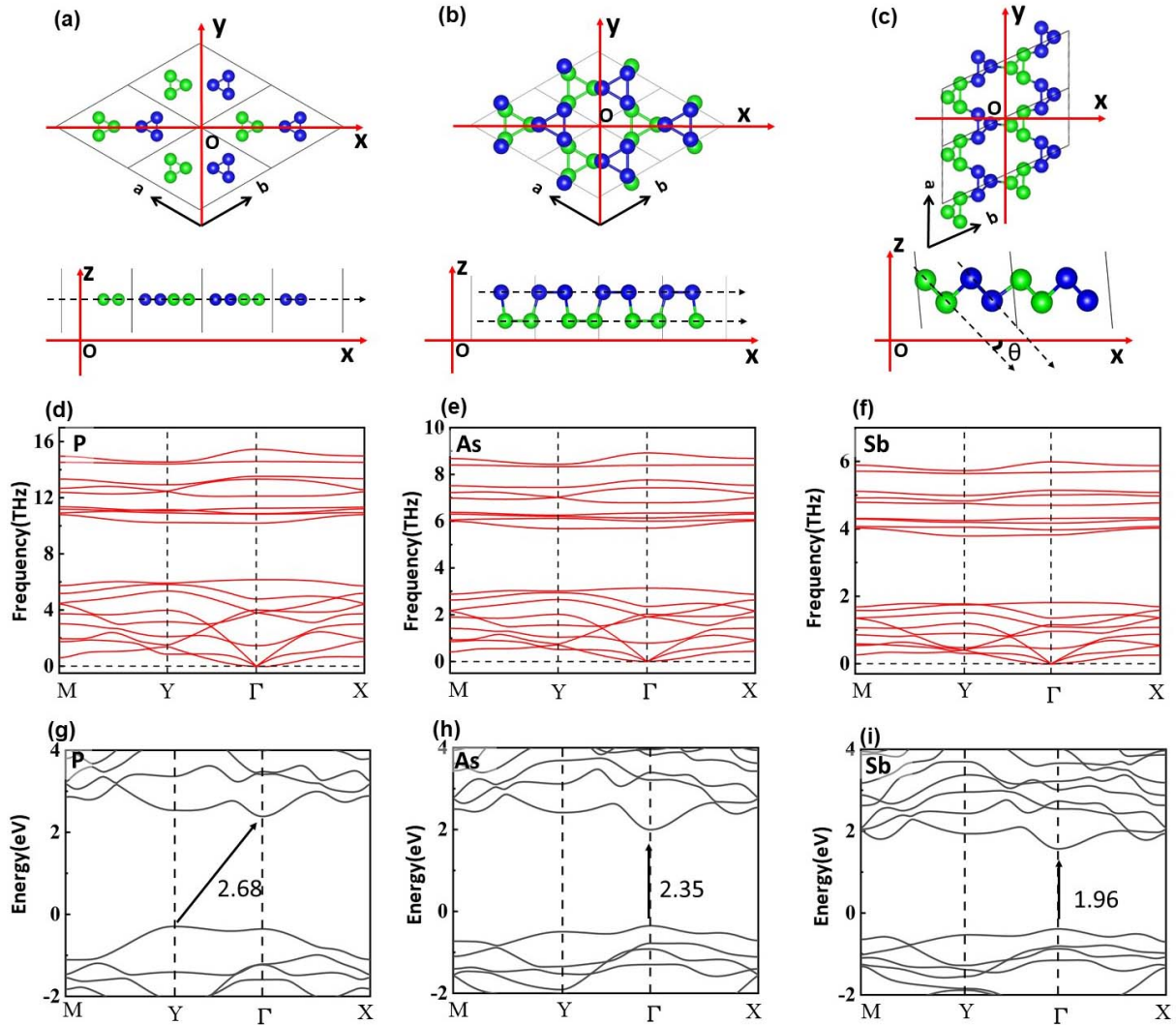


Figure S 4: Top and side views of different crystal structures. (a) Replacing each P-atom in a hexagonal lattice by P-trimer forming a kagome lattice. Two inequivalent trimers are distinguished by different color. (b) One P-trimer moves up and the other moves down to forming a buckled kagome lattice. (c) Each P-trimer rotate around x axis by θ to forming a tilted kagome lattice. The tilting angle $\theta=46.7^\circ, 43.1^\circ, 42.4^\circ$, for P, As and Sb, respectively. The bandstructures of phonon and electron are displayed in (d)-(i).

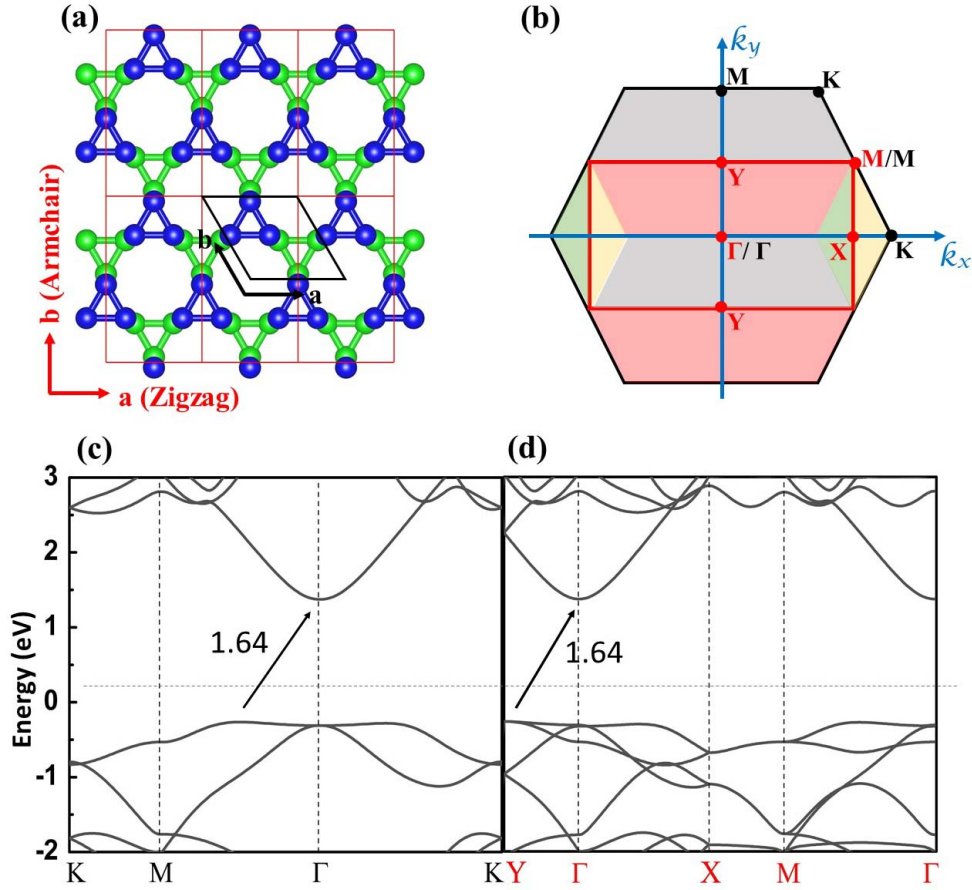


Figure S 5: Demonstration of band downfolding effect of kagome-P with different lattice choice. (a) The geometric structure of two lattices. The red line indicates the rectangular cell, the black line indicates the hexagonal lattice. (b) The Brillouin zones (BZs) for two lattices, the red rectangular box with red symbols is the BZ of the rectangular cell, and the black hexagonal box with black symbols is the BZ of the hexagonal cell. The former lies inside the latter. The color blocks inside the hexagonal BZ and meanwhile outside rectangular BZ can be downfolded into the rectangular BZ with the same color. (c) and (d) are the band structures of hexagonal and rectangular lattices, respectively. For instance, the highest valence band along ΓM in (c) will transform into the highest valence band along ΓY and the second highest valence band along $Y\Gamma$ in (d).

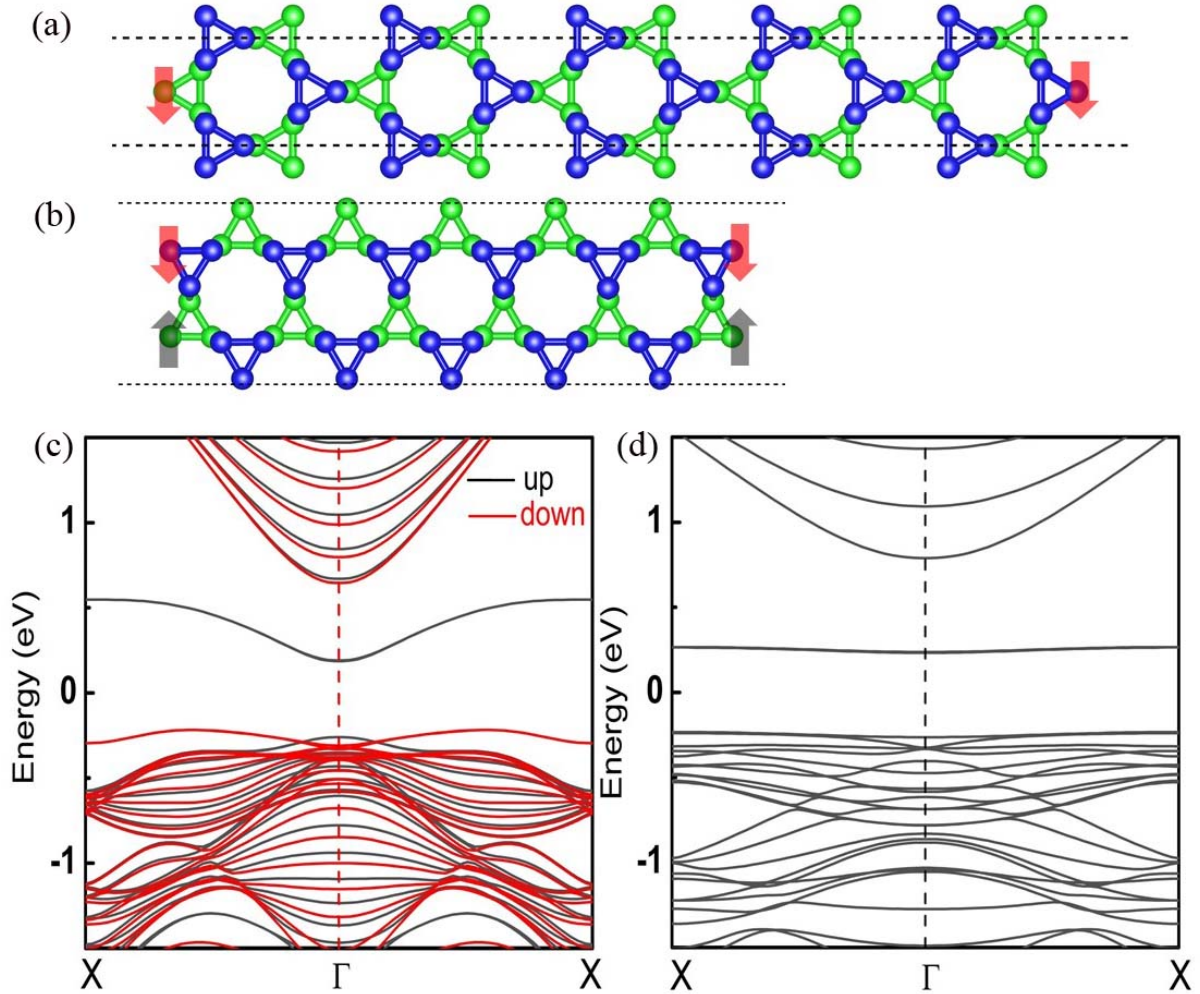


Figure S 6: Edge magnetism of kagome-P nanoribbon with dangling states. (a) For the zigzag nanoribbons, the intra-edge ferromagnetic and inter-edge ferromagnetic configuration is the ground state. (b) For the armchair ribbon, the intra-edge anti-ferromagnetic configuration is the ground state. The red and black arrows indicate the opposite magnetization directions on the outmost atoms. The band structures for (a) and (b) are exhibited in (c) and (d), respectively.